Comparative investigation of N donor ligand-lanthanide complexes from the metal and ligand point of view

T. Pruessmann, M. A. Denecke, A. Geist, J. Rothe, P. Lindqvist-Reis, M. Loeble, F. Breher, D. R. Batchelor, C. Apostolidis, O. Walter, et al.

Journal of Physics: Conference Series **430** (2013) 012115 doi:10.1088/1742-6596/430/1/012115

Comparative investigation of N donor ligand-lanthanide complexes from the metal and ligand point of view

T Prüßmann[1], MA Denecke[1], A Geist[1], J Rothe[1], P Lindqvist-Reis[1], M Löble[1], F Breher[1], DR Batchelor[1], C Apostolidis[5], O Walter[5], W Caliebe[2], K Kvashnina[3], K Jorissen[4], JJ Kas[4], JJ Rehr[4], T Vitova[1]

[1] Karlsruhe Institute of Technology (KIT), P.O. Box 3640, D-76021 Karlsruhe, Germany
[2] HASYLAB at DESY, Notkestr. 85, 22603 Hamburg, Germany
[3] European Synchrotron Radiation Facility, BP 220, F-38043 Grenoble Cedex, France
[4] Department of Physics, University of Washington, Seattle, WA 98195-1560, USA
[5] Institute for Transuranium Elements, European Commission, Joint Research Center, D-76125 Karlsruhe, Germany

E-mail: Tim.Pruessmann@kit.edu

Abstract. N-donor ligands such as *n*-Pr-BTP (2,6-bis(5,6-dipropyl-1,2,4-triazin-3-yl)pyridine) studied here preferentially bind An(III) over Ln(III) in liquid-liquid separation of trivalent actinides from spent nuclear fuel. The chemical and physical processes responsible for this selectivity are not yet well understood. We present systematic comparative near-edge X-ray absorption structure (XANES) spectroscopy investigations at the Gd L_3 edge of $[GdBTP_3](NO_3)_3$, $[Gd(BTP)_3](OTf)_3$, $Gd(NO_3)_3$, $Gd(OTf)_3$ and N K edge of $[Gd(BTP)_3](NO_3)_3$, $Gd(NO_3)_3$ complexes. The pre-edge absorption resonance in Gd L_3 edge high-energy resolution X-ray absorption near edge structure spectra (HR-XANES) is explained as arising from $2p_{3/2} \rightarrow 4f/5d$ electronic transitions by calculations with the *FEFF9.5* code. Experimental evidence is found for higher electronic density on Gd in $[Gd(BTP)_3](NO_3)_3$ and $[Gd(BTP)_3](OTf)_3$ compared to Gd in $Gd(NO_3)_3$ and $Gd(OTf)_3$, and on N in $[Gd(BTP)_3](NO_3)_3$ compared to *n*-Pr-BTP. The origin of the pre-edge structure in the N K edge XANES is explained by density functional theory (DFT) with the *ORCA* code. Results at the N K edge suggest a change in ligand orbital occupancies and mixing upon complexation but further work is necessary to interpret observed spectral variations.

1. Introduction

One of the major steps in the partitioning and transmutation (P&T) strategy for reduction of the longterm radiotoxicity of spent nuclear fuel is the separation of $5f$ elements from their chemically similar $4f$ counterparts. This separation is necessary, as the lanthanide (Ln(III)) fission products have large neutron absorption cross sections and thereby compromise transmutation efficiency in the nuclear fission process. Selective liquid-liquid extraction of actinides (An(III)) from Ln(III) has been demonstrated using soft donor extracting agents such as heterocyclic N-donor ligands, e.g., bistriazinylpyridines (BTP) [1] and bistriazinylbipyridines (BTBP) [2] with separation factors (SF) for Am(III) over Eu(III) greater than 100 (SF = distribution ratio D_{Am}/D_{Eu}; $D_M = [M]_{org}/[M]_{aq}$). Optimization of the partitioning ligands is a topic of global interest, as

the present ligands do not yet fulfill all criteria for application in an industrial process. Such optimization implies basic understanding of the chemical and physical processes responsible for ligand selectivity for *An*(III) over *Ln*(III). It was shown that BTPs act as tridentate ligands, forming 1:3 complexes with *An*(III) and *Ln*(III) in the solid state and in organic solution [3, 4]. Spectroscopic data available demonstrate thermodynamically favored *An*(III) extraction from nitric acid solution into the organic phase over *Ln*(III). However, we found with extended X-ray absorption fine structure (EXAFS) spectroscopy only subtle structural differences between the $[An(\mathrm{III})(\mathrm{BTP})_3](\mathrm{NO_3})_3$ and $[Ln(\mathrm{III})(\mathrm{BTP})_3](\mathrm{NO_3})_3$ complexes in organic solution, which may not fully explain *An*(III)/*Ln*(III) selectivity [4, 5]. Additionally, the *Ln* elements exhibit a trend in selectivity as a function of their ionic radii [6]. Systematic comparative X-ray absorption near edge structure (XANES) spectroscopy investigations at the *Ln* L_3 edge and N K edge can help differentiate bonding mechanisms between *An* and *Ln* bound to different ligands and counter ions, e.g., molecular orbital energy differences and relative electronic populations. We present comparative Gd L_3 high-energy resolution (HR-) XANES and conventional N K edge XANES spectroscopy combined with quantum chemical calculations to investigate the electronic structure of Gd(III) complexes from both the metal and the ligand point of view.

2. Experimental

Samples were prepared by drying iso-propanol solutions of $Gd(NO_3)_3$ (2 mmol/L) and $[Gd(BTP)_3](NO_3)_3$ (2 mmol/L $Gd(NO_3)_3$, 10 mmol/L BTP (*n*-Pr-BTP (2,6-bis(5,6-dipropyl-1,2,4- triazin-3-yl)pyridine) unless noted otherwise) on appropriate substrates for measurement. This leads to a 40% excess of BTP in the complex solution to ensure the formation of 1:3 complexes. We dried 2 μl (N K-edge) and 10 μl (Gd L_3 edge) on pieces of aluminium foil (5x5 mm^2) and on plastic holders for the N K edge and Gd L_3 edge experiments, respectively. Powder samples of $Gd(CF_3SO_3)_3$ (CF_3SO_3=OTf) and $[Gd(BTP)_3](OTf)_3$ were measured as pellets by mixing and pressing 2 mg compound with 20 mg cellulose. HR-XANES spectra at the Gd L_3 edge (7243 eV) were collected at the W1 beamline (HASYLAB) and ID26 beamline (ESRF). Incident X-rays were tuned to energies from 40 eV below to 70 eV above the Gd L_3 edge. The X-rays emitted from the sample were energy analyzed by a Johann spectrometer in dispersive geometry (W1) [7] or scanning geometry (ID26) [8] and were detected by a CCD camera (W1) or avalanche photodiode (ID26). The Lα_1 emission line (6053.4 eV) was diffracted and focused by one spherically bent Si(333) (W1) or Ge(333) (ID26) crystal with a 1 m radius of curvature at a Bragg angle $\theta = 78.4°$ (W1) or $\theta = 70.15°$ (ID26). N K edge spectra were measured at the UE52-PGM beamline (BESSY) using partial electron yield detection. A PGM (Plane Grating Monochromator) with a 1200 l/mm grating was used to tune the incident X-Rays from 380-420eV. The $[Gd(BTP)_3](OTf)_3$ spectrum and the *f* and *d* angular momentum projected density of states (*f*-, *d*-DOS) were calculated using the ab initio multiple scattering theory based *FEFF9.5* code [9]. The selfconsistent field (SCF card) and full multiple scattering (FMS card) calculations were performed on a cluster of 152 atoms corresponding to one $[Gd(BTP)_3](OTf)_3$ molecule. A Hedin-Lundqvist type exchange potential was used. The *f*-electron DOS was calculated self-consistently by using the UNFREEZEF card. The Fermi level was set to 3 eV below the calculated value of -9.6 eV in order to reproduce the pre-edge structure in the spectrum. To reach convergence, the core-hole type was set to random phase approximation (RPA card) and the core-hole potential was calculated for a cluster of 47 atoms (SCREEN card). The N K and Gd L_3 edge spectra were modeled with an arctangent function for the edge step and PseudoVoigt (PV) functions for all other features using the WINXAS software [10]. The shape parameter α of the PseudoVoigt functions was set to 0.5 to account for both experimental and core-hole lifetime broadening effects. Time dependent density functional theory (TD-DFT) calculations of the N K edge of H-BTP were performed using the *ORCA* package [11] with a def2-TZVP basis set, B3LYP functional, RIJCOSX SCF approximation and ZORA as scalar

relativistic approximation.

3. Results and discussion

3.1. Gd L_3 edge

Gd L_3 edge HR-XANES spectra of $[Gd(BTP)_3](NO_3)_3$ and $Gd(NO_3)_3$ are shown in figure 1 a. The $[Gd(BTP)_3](NO_3)_3$ spectrum is shifted 0.4 eV to lower energies compared to the $Gd(NO_3)_3$ spectrum indicating greater cation charge in the $[Gd(BTP)_3](NO_3)_3$ complex. This trend is preserved if NO_3^- is exchanged with an OTf^- anion. The $[Gd(BTP)_3](OTf)_3$ and $Gd(OTf)_3$ spectra are plotted in figure 1 b showing a 0.5 eV energy shift of $[Gd(BTP)_3](OTf)_3$ to lower energies. The additional pre-edge intensity at about 7241 eV, more noticeable for $[Gd(BTP)_3](NO_3)_3$ compared to $Gd(NO_3)_3$, can be assigned to $2p_{3/2}$ photoelectron transitions to $4f$ and $5d$ final states. The good experimental energy resolution of the ID26 data allowed us to model the WL and pre-edge areas (not shown here) and quantify the energy difference between these two resonances to be 0.4 eV smaller in the $[Gd(BTP)_3](OTf)_3$ than in the $Gd(OTf)_3$ spectrum. The origin of the pre-edge feature is revealed by calculations with the *FEFF9.5* code. The calculated $[Gd(BTP)_3](OTf)_3$ spectrum and the f-, d-DOS are plotted in figure 1 c. The f-DOS has high intensity at the energy position of the pre-edge feature suggesting that this feature arises from a mixture of $2p \rightarrow 4f$ and $2p \rightarrow 5d$ electronic transitions; however, the $4f$ contribution dominates. Even though the direct bonding partners of Gd change from N in $[Gd(BTP)_3](OTf)_3$ to O in $Gd(OTf)_3$, hardly any difference between the areas of the pre-edges and WLs is detectable, indicating that the relative electronic populations of the Gd $4f$ and $5d$ states are not significantly influenced by bonding with the n-Pr-BTP molecule. Nevertheless, the -0.4 eV relative energy shift and the 0.4 eV decrease in the energy difference between pre-edge and WL for $[Gd(BTP)_3](OTf)_3$ over $Gd(OTf)_3$ are clear indications for better screening of the $2p$ core-hole due to higher charge density on Gd in $[Gd(BTP)_3](OTf)_3$ than in $Gd(OTf)_3$. Future studies will investigate additional $Ln(BTP)_3$ and $An(BTP)_3$ compounds to obtain relative energy positions and oscillatory strengths of $2p_{3/2} \rightarrow 4f/5f$ and $2p_{3/2} \rightarrow 5d/6d$ electronic transitions, which might be correlated with BTP extraction properties.

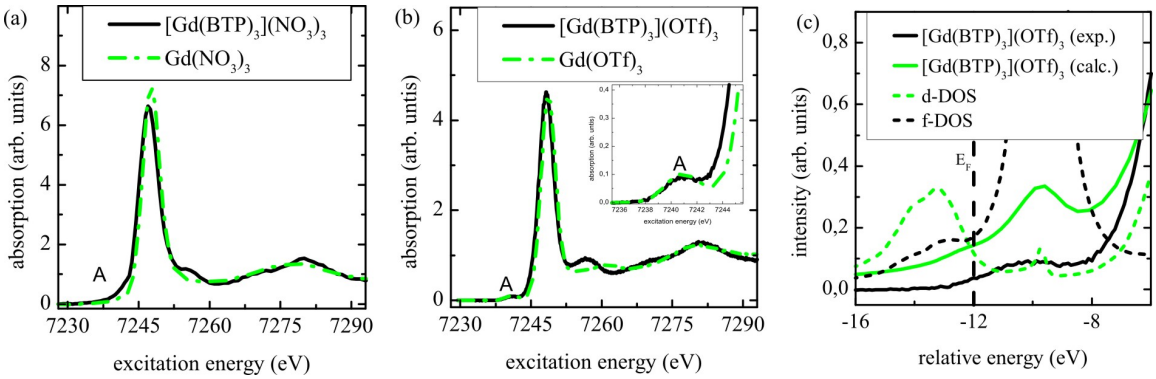

Figure 1. Gd L_3 edge HR-XANES spectra of (a) $[Gd(BTP)_3](NO_3)_3$ & $Gd(NO_3)_3$, (b) $[Gd(BTP)_3](OTf)_3$ & $Gd(OTf)_3$. Pre-edge calculated with *FEFF9.5* for (c) $[Gd(BTP)_3](OTf)_3$, including Gd f-, d-DOS.

3.2. N K edge

The N K edge XANES spectra a show a distinct pre-edge at about 399 eV (figure 2) arising from excitations of the N $1s$ electron to antibonding π^* orbitals. This feature can be successfully modeled with three PV functions. The $[Gd(BTP)_3](NO_3)_3$ pre-edge feature is shifted 0.1 eV

to lower energies compared to the BTP, suggesting higher charge density on N in the complex (better screening of antibonding π^*; see figure 2 b). The energy difference between features 1 and 2 is 0.52 eV and 0.46 eV in the $[Gd(BTP)_3](NO_3)_3$ and the BTP spectra, respectively, and feature 1 has 25% lower intensity (area) compared to feature 2 in the $[Gd(BTP)_3](NO_3)_3$ compared to the BTP spectrum, which indicates variations in orbital mixing and occupancies. In figure 2 b, feature 3 is better resolved in the BTP spectrum. However, we noticed a dependence on exposure time for this feature indicating that this part of the spectrum is susceptible to radiation damage. The theoretical N 1*s* spectrum of H-BTP calculated with TD-DFT (see figure 2 c) is shifted about 13 eV to lower energies, due to the omission of corehole and relativistic effects and to approximations used in the functional [12]. The calculated excitation bands are grouped around three energy positions representing the three features observed in the measurement. Each band can be described as a mixture of excitations into the LUMO (lowest unoccupied molecular orbital) and LUMO+1 and +2. These orbitals are localized on all N atoms of the ligand, which makes it difficult to distinguish between the different Gd-N metal-to-ligand bonds and to make any conclusions about their properties (e.g., orbital mixing and charge transfer). In future studies, we hope to overcome these difficulties by investigating several structural motifs of the BTP architecture (e.g., the pyridyl or triazine moiety [13, 14]) and *f*-element complexes thereof.

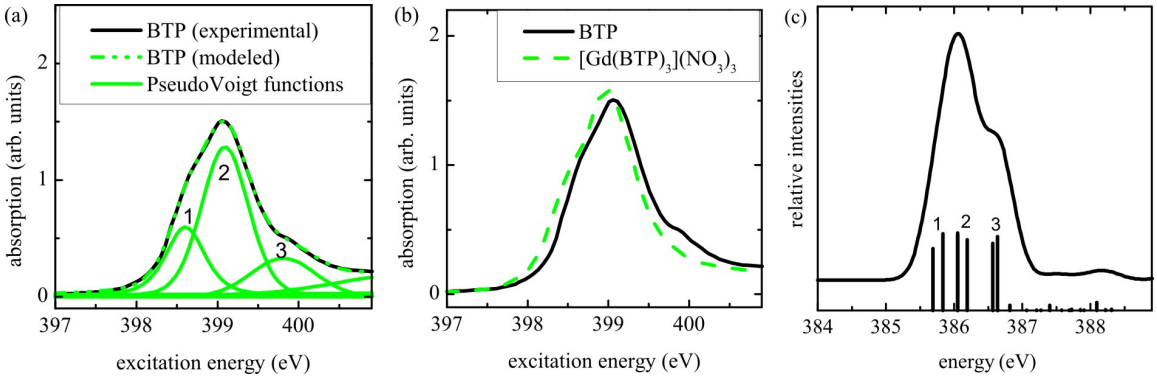

Figure 2. (a) an example of the pre-edge of N K edge XANES pre-peak modeled with PV; (b) N K XANES pre-peak of BTP and $[Gd(BTP)_3](NO_3)_3$; (c) TD-DFT calculation of N K H-BTP spectrum.

4. Conclusions

By performing quantum chemical calculations with the *FEFF9.5* code, we showed that the *Ln* L_3 HRXANES pre-edge feature in the $[Gd(BTP)_3](OTf)_3$ spectrum originates from a mixture of $2p rightarrow 4f$ and $2p \rightarrow 5d$ electronic transitions. Additionally, the 0.4 eV energy shift and the reduction in energy difference between pre-edge and WL by 0.4 eV in the $[Gd(BTP)_3](OTf)_3$ spectrum (see figure 1 b) indicated higher electronic density on the Gd in $[Gd(BTP)_3](OTf)_3$ compared to $Gd(OTf)_3$. No significant differences in electronic population of $4f$ and $5d$ states were detected for these materials. TD-DFT calculations of the N K pre-edge showed that the three absorption resonances associated with the pre-peak near 399 eV are due to 1s electron excitations to the LUMOs localized on all N atoms and that specialized investigations on single structural and chemical motifs are necessary to interpret variations in orbital mixing and charge transfer resulting from complexation of the ligand by an *f*-element.

Acknowledgments
We gratefully acknowledge KIT and Helmholtz Association of German Research Centers for financial support (VH-NG-734). This work is partially funded by the German Federal Ministry of Education and Research (BMBF) under contracts 02NUK020A, 02NUK012A and 02NUK012D. We thank HASYLAB, BESSY and ANKA for the granted beamtime.

References
[1] Kolarik Z, Mullich U and Gassner F 1999 *Solvent Extraction and Ion Exchange* **17** 1155–1170
[2] Geist A, Hill C, Modolo G, Foreman M R S J, Weigl M, Gompper K and Hudson M J 2006 *Solvent Extraction and Ion Exchange* **24** 463–483
[3] Drew M, Guillaneux D, Hudson M, Iveson P, Russell M and Madic C 2001 *Inorganic Chemnistry Communications* **4** 12–15
[4] Denecke M, Rossberg A, Panak P, Weigl M, Schimmelpfennig B and Geist A 2005 *Inorganic Chemnistry* **44** 8418–8425
[5] Banik N L, Schimmelpfennig B, Marquardt C M, Brendebach B, Geist A and Denecke M A 2010 *Dalton Transactions* **39**(21) 5117–5122
[6] Steppert M, Walther C, Geist A and Fanghanel T 2009 *New Journal of Chemistry* **33**(12) 2437–2442
[7] Welter E, Machek P, Drager G, Bruggmann U and Froba M 2005 *Journal Of Synchrotron Radiation* **12** 448–454
[8] Glatzel P, Sikora M, Smolentsev G and Fernández-García M 2009 *Catalysis Today* **145** 294 – 299
[9] Rehr J J, Kas J J, Prange M P, Sorini A P, Takimoto Y and Vila F 2009 *Comptes Rendus Physique* **10** 548 – 559
[10] Ressler T 1998 *Journal Of Synchrotron Radiation* **5** 118–122
[11] Becker U, Ganyushin D, Hansen A, Liakos D, Kollmar C, Kossmann S, Petrenko T, Reimann C, Riplinger C, Sivalingam K, Wezisla B and Wennmohs F 2010 *ORCA - An Ab Initio, DFT and Semiempirical electronic structure package* v2.8 ed
[12] Martin R L and Shirley D A 1977 *Many-electron theory of photoemission - Electron Spectroscopy, Theory, Techniques and Applications* vol 1 (Academic Press)
[13] Girnt D, Roesky P W, Geist A, Ruff C M, Panak P J and Denecke M A 2010 *Inorganic Chemnistry* **49** 9627–9635
[14] Bremer A, Geist A and Panak P J 2012 *Dalton Transactions* **41** 7582–7589